Indian Journal of Chemistry
Vol. 64, February 2025, pp. 172-182
DOI: 10.56042/ijc.v64i2.15263

Controlling macromolecular superstructures of AIE-active porphyrin by manipulating *p*H in water

Nilesh M Gosavi[a], Salman A L Shaikh[b], Latesh K Nikam[a] & Sheshanath V Bhosale*[b]

[a] Department of Chemistry, Baburaoji Gholap College, Sangvi, Pune 411 027, Maharashtra, India

[b] Department of Chemistry, School of Chemical Sciences, Central University of Kalaburagi, Karnataka 585 367, India

E-mail: bsheshanath@cuk.ac.in, latesh.nikam@gmail.com

Received 23 November 2024; accepted (revised) 22 January 2025

Supramolecular superstructures are controlled by *p*H dependent self-assembly of octaphosphonatetetraphenyl-porphyrin-**1** (**OPP-1**) in aqueous solution. UV-Vis absorption spectroscopy shows decreasing in the intensity of **OPP-1** in the *p*H range 3.0 to 6.0, which is correlated to *H*-type aggregates. However, absorption shifts to bathochromic (red-shift) under the influence of *p*H 8.0-11.0 range, which is typical for a *J*-type aggregate in absorbance spectrum as a result of supramolecular self-organisation constructed as compared to free **OPP-1** (molecules transitioned to a monomeric positions). In these, the **OPP-1** aggregated outside the surface *p*H 8.0-11.0 range is similar to growth of worm-like micelles. However, at *p*H range 3.0-6.0, **OPP-1** is aggregated inside the surface. Self-assembled **OPP-1** have been visualised on silicon wafer by Scanning Electron Microscopy (SEM), and it clearly shows that petite rod-like aggregates are formed at *p*H 5.0 and 6.0. Interestingly, **OPP-1** assemble into directional growth to produce worm-like micelle aggregates at *p*H 8.0 and 9.0, respectively. The main driving force of assembled supramolecules are basically based on *H*-bonding and stacking between central core of porphyrin. Finally, Dynamic Light Scattering (DLS) study supports mode of aggregation of short rods and growth of worm-like micelles in basic *p*H and X-ray diffraction (XRD) study clearly demonstrates that self-assembled structures are crystalline in nature. This interesting *p*H-dependent self-assembly phenomenon is based on **OPP-1** (synthetic analogue to natural occurring porphyrins) and can provide basis for development of novel conducting materials as well as biomaterials in the future.

Keywords: Supramolecular structures, Worm-like micelles, AIE-active aggregates, Scanning Electron Microscopy, Dynamic Light Scattering, X-Ray diffraction

Growth of wormlike micelles and other enormous supramolecular self-assembled structures has been observed in solutions containing single surfactant: non-ionic[1,2] zwitterionic[3], and ionic in the presence of added salt[4]. But, the growth of large micellar gathered usually detected in mixed surfactant solutions[5]. Upon the variation of solution's produces giant entangled wormlike micelles and their size and shape transformations[6]. The control of micelle growth from concentrated surfactant solutions is of primary importance for the personal-care and house-hold detergency[7] and also in applications of wormlike micelles in the oilfield industry[8]. Growth of wormlike micelles from non-ionic surfactant in solutions have been reviewed by Pelan and co-workers[9]. The fabrication of highly ordered nanostructures of chromophores *via* self-assembly is an active area of research with diverse applications in materials science. The construction of functional artificial systems *via* self-assembly of naturally occoring porphyrins by non-covalent interactions employing *H*-bonding, hydrophobic, dipole-dipole, van der Waals interaction, π-π stacking, and solvophobic interactions is an alternate approach[10]. To achieve the precise arrangement of the monomers in a dynamic and thermodynamically stable structures, the vigilant design of the chromophore with specific molecular recognition sites are required. Porphyrins, particularly natural *i.e.*, chlorophylls and/or protoporphyrin-IX and their derivatives, consist of a hydrophobicity, rigidity, apolar and polar part to their substitution patterns[11], which make their important characteristic because of this arrangement it prevents crystallization and favourable for self-aggregation[12]. These attractive chromophores and their derivatives useful for creating various superstructures for mimicking light harvesting (LH-1 and LH-2) systems[13]. Since porphyrins attractive features, researchers are interested to develop supramolecular self-assemblies for polymeric porphyrin wires for long range energy

and electron transport[14]. In difference, symmetric tetraphenylporphyrins (TPPs) lack this diversity of functional groups and have a high tendency to crystallize. However, water-soluble symmetric TPP derivatives[15], formed nanostructures or form well-defined Langmuir-Blodgett monolayers on smooth solid surfaces[16]. Water soluble TPP derivatives bearing long side chains with water-soluble groups produces fibrile structures at low *p*H [17]. Fuhrhop and co-workers also developed phosphonatoporphyin as building blocks for to build tower-like structures on silicon as well as gold electrodes for electrochemically, in which they have chosen zirconium-(IV) as cement between phosphonate groups and led to broad rocks, instead ill-defined monomolecular aggregation[18]. Typically, using irreversible or reversible self-assembly procedures yield robust zirconium (IV)-porpyrinphosphonate cones in μm-long fibers of monomolecular thickness. In these directions, De Napoli *et al.* found that self-assembly of phosphonatoporphyrin with more flexible chains was demonstrated to be formation of hierarchical ill-defined monomolecular aggregation in aqueous solution[19]. However, there are limited reports of porphyrin assembled into micellar superstructures with defined lengths and dimensions from charged and amphiphilic porphyrins[20,21]. Fuhrhop group, in another report explored novel porphyrin (meso-tetrakis-[(bixinylamino)-o-phenyl] porphyrin) derivative functionalized with four cartenoid *i.e.* bixin substituted at periphery, which spontaneously formed vesicular aggregates in water at *p*H = 9 can remain essentially intact even on dry solid surfaces because of non-specific intermolecular interactions and π-π stacking of the core porphyrins[22]. Porteu *et al.*[23] and Bai group[24] studies on the anionic substituent are anticipated for the further described self-assembly of porphyrins using zwitterionic *via* *J*-aggregate construction, in which electrostatic interactions amongst the positively charged porphyrin core and the negatively charged groups through molecular recognition with specific *H*-bonding. However, these types of studies are still limited and researchers are working towards further development to produce decent conducting materials as well as biomaterials in future developments.

Results and Discussion

To develop further, we have synthesis 5,10,15,20-tetrayltetrakis[(benzene-5,1,3-triyl)bis(12 microscopy (Fig. 1: **I**) 25. The self-assembly were modulated by intermolecular *H*-bonding of the amino groups of cyclam molecules with phosphonates moieties along with hydrophobic interactions with porphyrin core of the **OPP-1** produces long wires[25]. In another report, supramolecular self-assembly of an **OPP-1** with three nucleobases, namely: adenine, cytosine, and thymine are studied (Fig. 1: **II**)[26]. Typically, **OPP-1** with 8 equiv. of cytosine produces light-harvesting ring-like structures, which is similar to those observed in

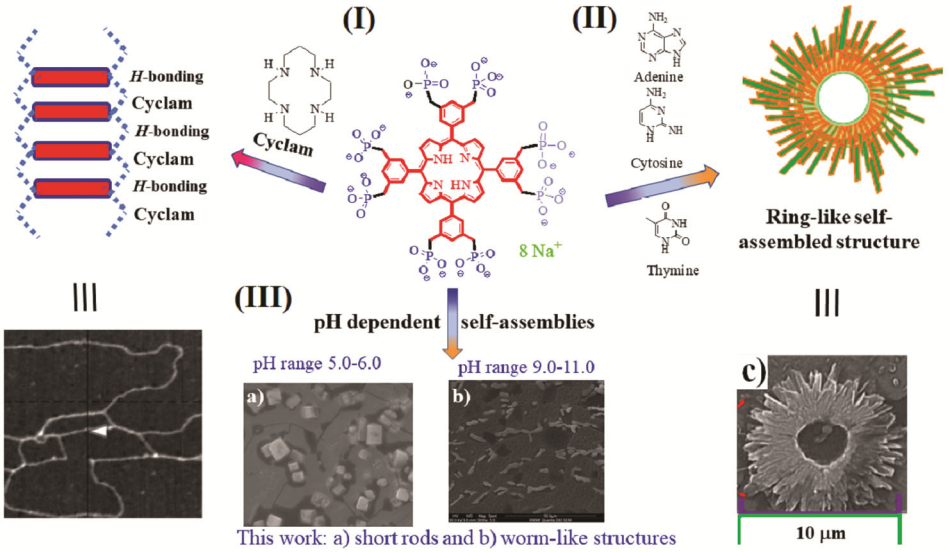

Fig. 1 — Molecular arrangement: (**I**) cyclam, **OPP-1** in the presence of cyclam self-assembled into nano-wire morphology, (**II**) **OPP-1** with 8 equiv. of three various nucleobases namely: Adenine, Cytosine and Thymine, respectively, and (**III**) in this study, various supramolecular self-assembled structures were formed such as micellar rod-like (at *p*H = 3.0 to 6.0), micellar particular aggregates (at *p*H = 8.0) and micellar worm-like (at *p*H = 9.0) structures with variable *p*H in water, respectively.

natural light-harvesting antenna-like fractal growth. However, porphyrin assembled with adenine or thymine resulted in prisms and microrods, respectively. Scanning Electron Microscopy (SEM) used to visualize the self-assembled nanostructures and their behaviour in the solid state. This study demonstrated a deeper understanding on how one can employ donor/acceptor subunits in supramolecular assemblies to construct artificial architecture. However, absorption shifted to bathochromic (red-shift) under the influence of *p*H 8.0-11.0 range, which is typical for a *J*-type aggregates in absorbance spectrum as a result of supramolecular self-organisation constructed as compared to free **OPP-1** (molecules transitioned to a monomeric positions), in which **OPP-1** aggregated outside the surface *p*H = 8.0-11.0 range similar to growth of worm-like micelles. However, at *p*H range 3.0-6.0, **OPP-1** aggregated within the surface[27,28].

In this study, we report for the first-time use of **OPP-1** (Fig. 1: **III**), for *p*H dependent self-assembly with varying *p*H ranging from 3.0-11.0 in aqueous solutions, the displacement of peripheral anionic phosphonate functional groups of **OPP-1** is shown to have a main consequence on the aggregation behaviour. UV-Vis absorption and fluorescence (FL) conducted to study optical and emission properties while Scanning Electron Microscopy (SEM) technique was used to study the nanostructured morphologies on the silicon surface.

UV-Vis absorption and fluorescence spectroscopy

Characteristically, AIE-active **OPP-1** is readily soluble in water at *p*H 7.0 and the identical to natural porphyrins, UV-Vis spectrum of **OPP-1** exhibits an intense Soret band at 418 nm ($\varepsilon = 2.56\times10^5$ L M^{-1} cm^{-1}), together with four weaker Q-bands at 510 (13.8), 540 (12.8), 575 (9.0), 635 (5.5) nm with 10^3 ε, M^{-1} cm^{-1} as shown in Fig. 2. It clearly indicates **OPP-1** does not produce any type of aggregates in in neutral *p*H and characteristically, tetraphenyl-porphyrin is known to absorb in the region around ~420 nm[29-31].

The UV−vis absorbance spectrum of **OPP-1**, in fact, at *p*H 5.0, the most prominent band in the absorption spectrum is slight red-shifted with respect to that of the species existing at basic *p*H 11.0 *i.e.* Soret band appeared at 445 (2.38). At *p*H 5.0 absorption of **OPP-1** displays Soret band 425 nm with vanishing of three Q-bands and appearance of blue-shifted one Q-band at from 575 nm to 515 nm. The appearances of such characteristic absorption bands indicate the formation of the planet-to-plane π-π stacking (hypsochromic shift), that indicates *H*-type aggregates and can be designated as formation of small assembly due to partial deprotonation form of **OPP-1** in acidic medium. The Soret band of the full deprotonated form *i.e.* *p*H ranging from 8.0-11.0, entitles **OPP-1** Soret band appeared at 440 nm (at *p*H 9.0) and 445 nm (*p*H 11.0), with appearance of new Q-band at 636 nm (22.0) along with other three red-shifted Q-bands at 525 (13.8), 545 (12.8), 583 (12.0), respectively, which is clearly reveals formation of *J*-type aggregates (Head-to-tail stacking *i.e.* bathochromic shift). From the UV-Vis absorption clearly shows formation of larger assembly at basic *p*H and small structures in aqueous acidic medium. Thus, absorption shifted to bathochromic (red-shift) under the influence of *p*H 8.0-11.0 range, which is

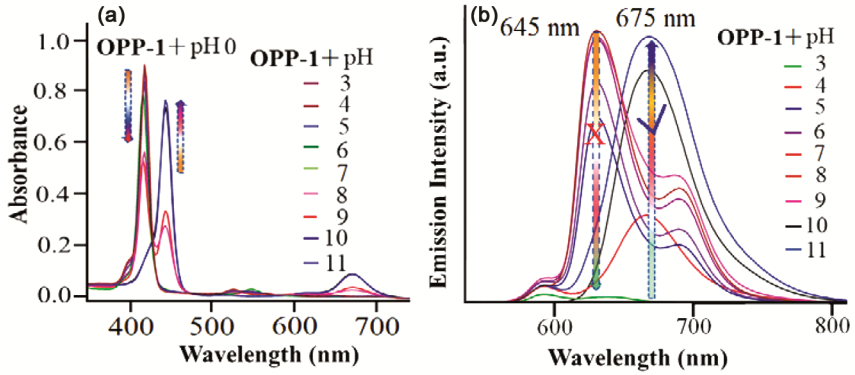

Fig. 2 — (a) UV-Vis absorption spectrum of **OPP-1** at concentration 1×10^{-4} M at *p*H values ranging from 3.0-11.0. Arrows in UV-Vis represents in the direction of increasing *p*H with acidic and basic aqueous solvent are specified in mol·L^{-1}, and (b) FL of **OPP-1** (1×10^{-4} M, λ_{ex} at interface of UV-Vis absorption *i.e.* at 425 nm. Dash arrows directs forbidden *H*-aggregates at acidic medium (quenching of FL was observed, *H*-type aggregated species) and in basic *p*H (*J*-type aggregated species) directional growth of assembly in aqueous medium is allowed, respectively.

typical for a *J*-type aggregates in absorbance spectrum as a result of supramolecular self-organisation constructed as compared to free **OPP-1** (molecules transitioned to a monomeric positions), in which **OPP-1** aggregated outside the surface *p*H 8.0-11.0 range similar to directional growth worm-like micelles. However, at *p*H range 3.0-6.0, **OPP-1** aggregated inside the surface[27,28] similar to inverse micellar structures.

Furthermore, FL of **OPP-1** was further examined in water and as usual typical two bands at 645 and very weak emission at 675 nm at *p*H =7.0 (λ_{max} = 425 nm) as demonstrated in Fig. 2b. In sharp contrast, the FL was decreases with decreasing *p*H = 3.0-6.0 with blue-shifted in addition the FL of **OPP-1** completely diminished, which also is typically observation for formation on small aggregates. which may be due to the partial protonation of phosphonate groups. In which **OPP-1** precipitation was observed from solution (greenish turbid solution of **OPP-1**, which can be seen by bare eyes). Interestingly, at basic (*p*H = 8.0-11.0), **OPP-1** FL shows red-shift, due to fully deprotonated peripheral phosphonate group, which due to self-organisation and directional growth *via* head-to tail fashion similar to Aggregation Induced Emission (AIE) fashion. The quantum yield of **OPP-1** in the fully protonated form at *p*H = 7.0 was shown to be 0.12 (at λ_{max} = 645 nm) which is comparable to standard reference tetraphenylporphyrin (Φ_F = 0.11)[32]. The quantum yield Φ_F = 0.12 decreases with decreasing *p*H from 7.0 to 3.0 *i.e.* Φ_F = 0.12 to 0.001 *i.e.* at *p*H = 3.0 fully diminished emission of **OPP-1** was observed with Φ_F = 0.001. While in basic *p*H = 11.0 increasing Φ_F with red-shit (675 nm) along with shoulder peak appeared at 655 nm was observed with Φ_F = 0.10, which is due to AIE-species formation *i.e.* J-type aggregated and comparable to self-assembled structures formed[25,26]. Important to mention that in basic medium the FL of **OPP-1** split into two peaks at 655 nm (weak emission) and 675 nm (AIE-species *i.e.* red-shifted emission to *p*H = 7.0), this split of FL was not only self-assembly formation but also AIE-effect[34-36]. Due to the fact that, there are limited electronic communication between porphyrin cores with in the network of *H*-bonding and van der Walls interactions and laterally with π-π stacking of core of the **OPP-1** (Fig. 2b) in basic aqueous medium and this behaviour is the complete opposite to the self-assembly of **OPP-1** in acidic medium. Thus, molecular aggregation alters the optical properties of a FL quenched. This is usually *H*-aggregates show non-FL, blue-shifted absorption bands with respect to the isolated monomer, *J*-aggregates are fluorescent displaying a red-shifted aggregates, similar to AIE-active fluorophores.

Table 1 clearly shows the effect of changing *p*H (5.0, 7.0, 9.0 and 11.0) has been investigated. The absence of the Soret band of the monomeric form *i.e.* fully protonated form strongly suggest that the higher aggregate presiding over the hierarchy is that formed at *p*H close to 8.0-11.0, respectively and quenching effect in fluorescence emission and slight shift of Soret band in acidic medium clearly indicates formation of small aggregates.

H-type and *J*-type aggregates of OPP-1

Unsurprisingly, the UV-Vis absorption and fluorescence spectroscopy clearly demonstrates *J*-type of aggregates at *p*H range 8.0-11.0 (Fig. 2). However, **OPP-1** in the *p*H range *p*H 3.0-6.0 demonstrates only decreasing of UV-Vis absorption and FL and is characteristically **OPP-1** aggregate in a plane-to-plane π-π stacks (parallel way) to form a sandwich-type arrangement called *H*-aggregate *i.e.* blue-shifted absorption (which is due to a higher energy transition) compared to the free monomeric **OPP-1** molecules as shown in Fig. 3[33]. As an alternative, the **OPP-1** assembled into head-to-tail prearrangement (end-to-end stacking), which is typically formation of *J*-aggregates *i.e.* red-shifted absorption (displaying lower transition energy) compared to the free dye as illustrated in Fig. 3. The exciton theory says that in the *H*-aggregates the fluorescence emission is forbidden, while *J*-aggregates are emissive The fluorescence emission is forbidden that in the *H*-aggregates which is due to exciton theory, while

Table 1 — UV-Vis absorption and fluorescence emission data of **OPP-1** under various *p*H conditions in aqueous solution

*p*H	Soret-band (λ, nm; 10^5 ε, M^{-1} cm^{-1})	Q-bands (λ, nm; 10^3 ε, M^{-1} cm^{-1})	emission (λ, nm)
7.0	418 (2.56)	510 (13.8), 545 (12.8), 578 (12.0), 626 (10. 6)	645, 675[a]
5.0	422 (1.4)	516 (9.6), 656 (36)	no[b]
9.0	440 (2.29)	534 (21.2), 594 (14.8), 644 (12.8)	655[a], 675[c]
11.0.0	445 (2.38)	516 (22.0), 559 (12.8), 583 (12.0), 636 (10.6)	655[a], 675[c]

[a] Very weak emission, [b] No emission and [c] Red-shift emission.

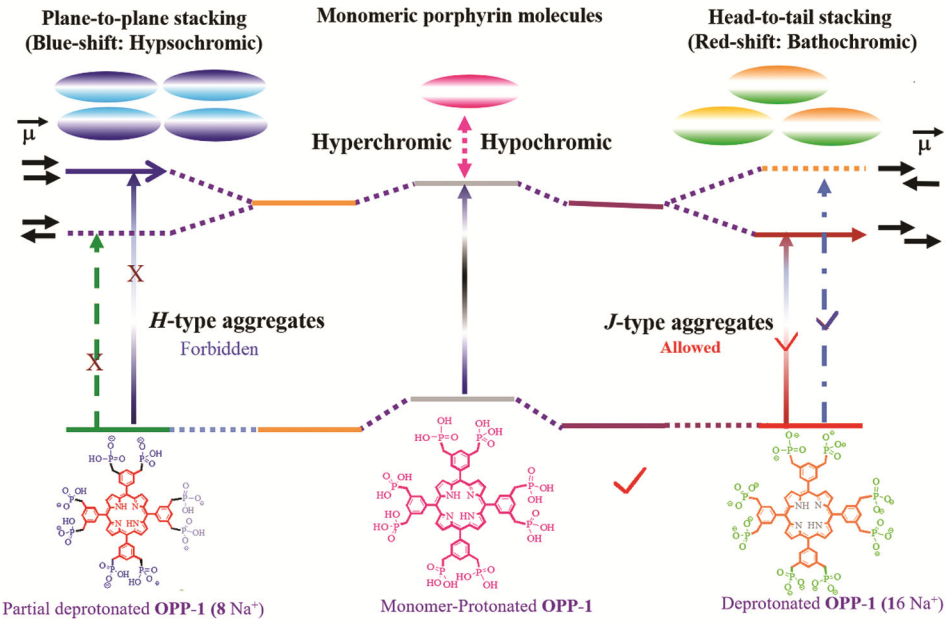

Fig. 3 — A *H*-aggregate is a type of **OPP-1** that shifts to a shorter wavelength (hypsochromic shift; which is forbidden process in partial protonated form of **OPP-1**) and *J*-aggregate **OPP-1** shifted to a longer wavelength (bathochromic shift; which is allowed process due to fully protonated form of phosphonate group), which is similar to AIE-active fluorophores, as a result of supramolecular self-assembly followed by superstructure organisation of **OPP-1** was yielded, respectively.

J-aggregates are emissive with red-shift[37], due to the attractive Coulomb interaction between the enthusiastic electron and the hole thus created binds them together to form a bound porphyrins within the two charge carriers such as a *H*-bonding.

Scanning electron microscopy (SEM) analysis

To understand mode of aggregation, Scanning Electron Microscopy (SEM) analysis was used, which clearly shows formation of various supramolecular well defined tunable nanostructures with minor changes in *p*H, which was confirmed by SEM tomography as shown in the Fig. 4, Fig. 5, Fig. 6 and Fig. 7. SEM was used to examine the morphology microstructures of the self-assembled **OPP-1** in the range *p*H = 3.0-11.0 deposited on a silicon wafer by spin coating and removing excess water by filter paper. In fully protonated form **OPP-1** does not yield any prominent assembly rather it produces only inflatable aggregates (Fig. 4), however, one cannot envisage correct length and width of self-assembled structures at *p*H = 7.0, because formed assemblies are flat on the silicon wafer.

Moreover, the partial deprotonated (in acidic medium) and fully deprotonated form of **OPP-1** clearly shows formation of various supramolecules, that indicates varying *p*H plays a vital role in keeping

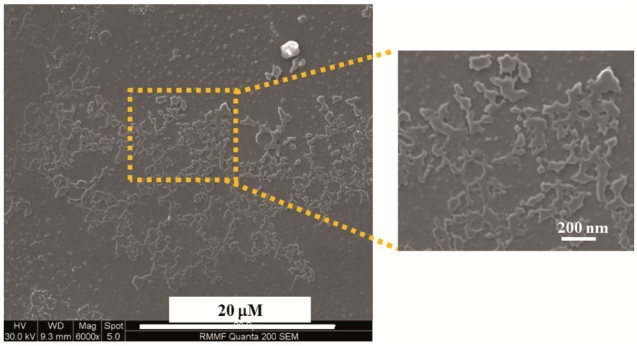

Fig. 4 — SEM micrographs of the supramolecular self-assembled structure of **OPP-1** (10^{-4} M) at *p*H = 7.0, which was deposited from aqueous medium on a silicon wafer by spin coating and removing excess water by filter paper. One can see that **OPP-1** in *p*H 7.0 produces flat inflatable aggregates due to protonated form, which made it difficult to measure size and shapes.

the **OPP-1** derivatives apart from each other in acidic aqueous medium after spin coating and removing excess solution[31]. In particular, **OPP-1** in acidic medium gives fractional deprotonated form *i.e.* eight negative charges at peripheral phosphonate functional group. As the phosphonate groups have pKa_1 = 3.0, and the acidic pyrrole subunits of the porphyrin core with pKa_2 = 5.6, while the second phosphonate proton having a pKa_3 value of 8.0. Therefore, in partial protonated form **OPP-1**, in acidic aqueous water (at *p*H = 5.0-6.0), thus, we hypothesise that, the **OPP-**

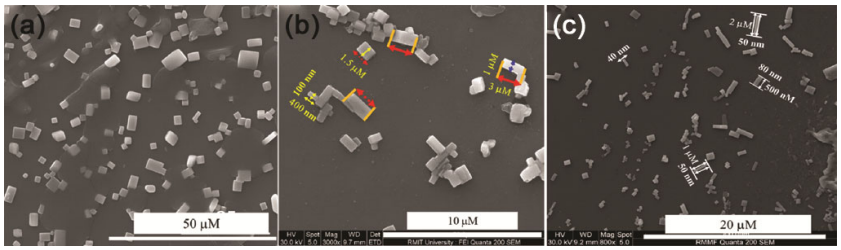

Fig. 5 — SEM images of the supramolecular self-assembly of **OPP-1** (10^{-4} M): (a) at *p*H = 6.0 (Scale bar = 50 µM), (b) enlarged SEM images (from 50 µM to 10 µM) to imagine size and shapes of the rod-like morphologies of a), and (c) assembled structures at *p*H = 5.0 (Scale bar = 20 µM), respectively. **OPP-1** produces rod-like morphology with diameter of about 40 nm up to 1 µM and length varies from 400 nm up to 3 µM, which significantly larger than the molecular dimension of **OPP-1** (*ca*. 2.4 nm).

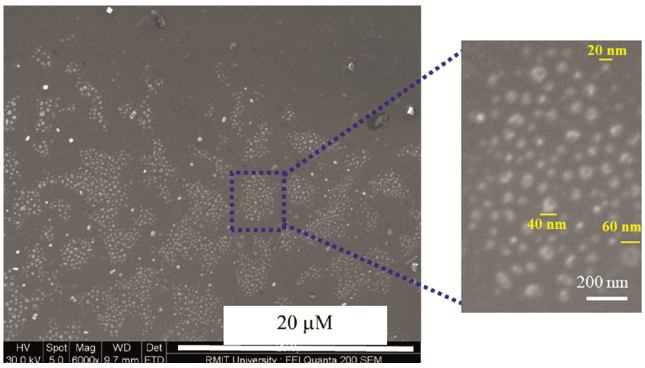

Fig. 6 — SEM images of **OPP-1** in basic (*p*H = 8.0) aqueous solution: a) supramolecular self-assembly of **OPP-1** from solution of 10^{-4} M produces invert spherical particular aggregates, and (b) shows enlarged particular aggregates of a), respectively. Scale bare of a) is 20 µM, and b) is 200 nm, respectively.

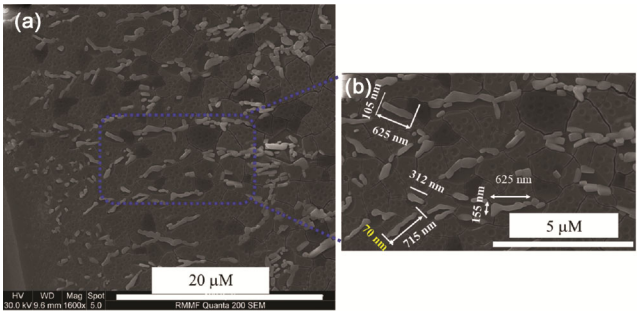

Fig. 7 — SEM micrographs of the supramolecular self-assembled superstructures formation: a) of **OPP-1** (10^{-4} M) at basic *p*H = 9.0 in aqueous medium. Non-covalent interactions between **OPP-1** in the plane *via* fully deprotonated phosphonate groups of **OPP-1** with water molecules upon spin coating on silicon wafer with removing excess basic aqueous solvents by using filter paper, and b) enlarged image of a), Scale bar is 20 µM a), and 5 µM in the b), respectively. From enlarge SEM images in b) clearly demonstrates size and shapes of micellar worm-like self-assembled superstructures with doubling and triplicating of the sizes of the worm-like structures.

1 molecules partially coordinate with the with two *H*-bonds on each side of the peripheral phosphonate moieties are first consumed to form the in-plane complex and produces micellar rod-like structures, in which micellar rods are aggregated form of partially charged molecules and are loosely held together through hydrogen bonds, electrostatic/solvophobic interactions of several hundreds of **OPP-1** molecules aggregates, is similar to water-in-oil system.

Typically, exposure of the hydrophilic phosphonate head groups of **OPP-1** energetically unfavorable but matches with the formation of inverse/reverse micellar rod-morphologies (Fig. 5)[37]. In the *p*H array 6.0, 5,0, 4,0 and 3.0 yielded detached micellar rod-structures in the *p*H = 6.0 and 5.0, however, **OPP-1** yielded dense short rods-structures combined together to form glued dense morphology as shown in ESI Figure S1, respectively. Static, **OPP-1** at (*p*H = 5.0 and 6.0 produces rod-like morphology with diameter of about 40 nm up to 1 µM and length of rod-like morphology fluctuates from 400 nm up to 3 µM in the both *p*H's = 6 and 5, which is similar to formation of self-assembled structure naphthalene diimide's in mixed polar and non-polar solvents[38] and significantly larger than the molecular dimension of **OPP-1** (*ca*. 2.4 nm). Nevertheless, at lowering the *p*H < 5.0 *i.e.* *p*H = 4.0 and 3.0, SEM shows formation of micellar rod-like morphology, however, rod-like structures tend to amalgamated together to form compact assemblies (See ESI Figure S1).

Remarkably **OPP-1** at *p*H = 8,0 produces micellar spherical particles as shown in Fig. 6, which is completely opposite to formation of rod-like morphology in the *p*H range from 6.0-3.0 (Fig. 5 and Figure S1). SEM imaging shows formation of micellar particular assembled structures with sizes ranging from 20, 40 and 60 nm as shown in Fig. 6. From SEM analysis, it can be seen that the reverse micellar particles size is higher than **OPP-1** (*ca*. 2.4 nm) and precise micellar particular self-assembled structures are doubling and tripling. SEM topographical images shown in Fig. 6, clearly shows that **OPP-1** may firstly produces particles in 20 nm

sizes which may further combined together to form 40 and larger 60 nm in sizes. Which in fact interesting to increase basic nature on self-assembly to see whether these particles are joint together to form other structures.

Thus, furthermore upon increasing *p*H from 8.0 to 9.0, in which **OPP-1** in the form of fully deprotonated *i.e*. 16 phosphonate groups of **OPP-1** induces head-to-tail arrangements (*J*-type aggregates) along with increasing quantum yield owed to AIE-effect[33,34]. In fully deprotonated phosphonate groups of **OPP-1** upon spin-cast on silicon wafer plate after the solvent was evaporated interact with water through *H*-bonding electrostatically and produced attractive features (Fig. 7a), which is producing micellar worm-like self-assembled superstructures aggregates with width of worm-like aggregates shown to be doubled and tripled *i.e*. 70, 105 and 155 nm and can be seen in enlarged Fig. 7b, respectively. SEM images shows formation of aggreges with length is about 312 nm, 625 nm and 715 nm, respectively, as revealed in Fig. 7b), important to mention that length of the micellar worm-like structures also doubling and triplicating. Also, it is demonstrated that, **OPP-1** cooperative together, thus, in some instances width and length were doubling and tripling in both acidic (*p*H 6.0 and 5.0; Fig. 6) and basic medium (*p*H = 9.0). Typically, in basic aqueous medium (*p*H = 9.0; Fig. 7), respectively. Furthermore, SEM images (as shown in Figure S2), which clearly limited directional growth. Which may be due to that fact that micellar worm-like structures of **OPP-1** accumulate together to form dense fibrils network at higher *p*H range *i.e*. *p*H 10.0-11.0 (See ESI, Figure S2a and S2b).

Nevertheless, it clearly recompenses of this approach over the simple precipitation self-assembly, which difficult to avoids the possibility to control the morphology into various supramolecular superstructures. **OPP-1** (10^{-4} M) produces micellar rod-like structures in acidic medium ranging from *p*H = 6.0 to 3.0 and micellar particles at *p*H 8.0. Furthermore, micellar particles tend to further joint together to yield micellar worm-like superstructures at *p*H = 9.0 with directional growth to produce attractive features. In addition, it can be seen from the SEMs images that the supramolecular assembled structures are completely distributed in acidic medium (partial deprotonated of phosphonate group of **OPP-1** at *p*H = 5.0 to 6.0 and also in basic medium (fully deprotonated of phosphonate groups at peripheral of **OPP-1**) *i.e*. at *p*H = 8.0 and 9.0. In these cases, **OPP-1** do not tend to associate with each other in both acidic and basic medium as shown in above Figs. 5-7. Thus, formation of micellar worm-like self-assembled structures with which one may study long lived charge separation by functionalization of core of the **OPP-1**.

The aggregation behavior of rod-like assemblies of **OPP-1** in aqueous solutions was investigated using UV–vis absorption and FL spectroscopy, and SEM analysis (the experiments herein were executed stabilizing 2 h prior to collect images from preparation of the assemblies in aqueous solutions of **OPP-1**. A pointedly FL quenched (*H*-type aggregates) in acidic aqueous medium due to the arrangement of the conjugate revert micellar rod segments and in basic aqueous medium micellar spherical particles at *p*H = 8.0 and worm-like morphology at *p*H = 9.0 was observed with AIE phenomenon of *J*-type aggregates. Thus, to confirm the hypothesis, DLS experiments further corroborated the assumption that **OPP-1** self-organize into ordered nanoaggregates with average indicating that the formation of nanofibers or large bundles is preferred over self-organization of micelles in aqueous solutions.

Dynamic Light Scattering (DLS)

Dynamic light scattering (DLS) used to determine photon correlation spectroscopy (PCS) and is a very powerful tool for studying the dispersion behaviour of macromolecules in solution. The diffusion PCS measures hydrodynamic radii in nm depends on the size and shape of macromolecules produced from **OPP-1**. DLS technique is a fast, non-invasive, specific, reliable and auspicious technology which is well predictable for size measurement and study of size distribution of molecules in submicron ~10 μm to 1 nm with having molecular weight <1000 Dalton. Thus, in this study, we provide practicality of DLS to study the homogeneity of sizes in solution of π-π stacking of the porphyrin core as well as to study assembled structures by protonated form of the phosphonate group of **OPP-1** molecular interactions. In DLS dimension m, it is important key to control *p*H's, when performing experiments in dilute aqueous medium, as it can often sizes of assembly speciously conc. Size distributions from DLS for actually depending on self-assembled and molecular weight of the molecules, as usually if one cannot control *p*H's may produces repulsions between monomers are no

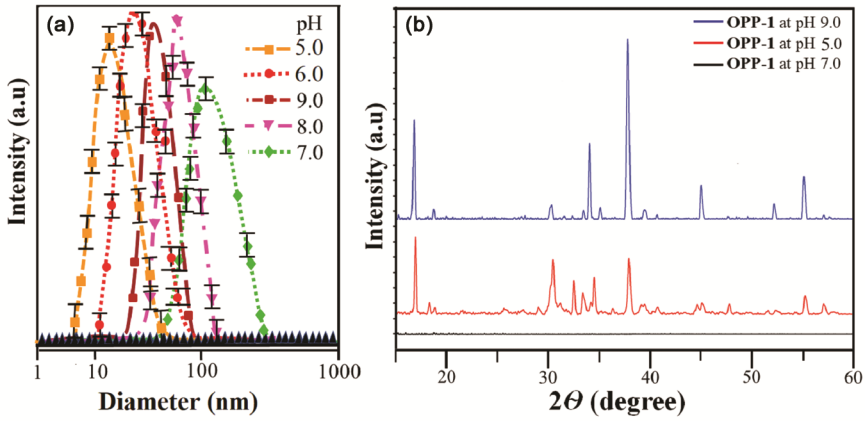

Fig. 8 — (a) Dynamic Light Scattering (DLS) of **OPP-1** (10^{-4} M) at three different *p*Hs = 9.0, 7.0 and 5.0, in aqueous solutions, respectively, reveals formation of the self-assembled structures in solution with varying sizes, and (b) X-Ray Diffraction (XRD) of **OPP-1** pattern on amorphous silica signifying shows formation of amorphous to crystalline nature of morphology on the surface with varying *p*H from aqueous solution: at *p*H 7 (black-curve) shows amorphous nature, assembled structure at *p*H 5.0 (red-curve) produces broad peaks with crystalline in nature, and self-assembled superstructure at *p*H = 9 (blue-line) produces sharp-peaks, which is similar to crystalline nature of superstructure of **OPP-1**, respectively.

longer divided, and the normally broad DLS peaks observed. At sophisticated *p*H's in both acidic and basic medium this effect becomes bottled-up approach producing better DLS peaks. It can be seen in Fig. 8a, DLS clearly demonstrates formation of self-assembled structures in aqueous solution. It can be seen, the diameter determined at *p*H = 5.0 shows formation of 210 nm and at *p*H = 6.0 produces 450 nm diameter in sizes in acidic aqueous medium. However, in basic *p*H at 9.0 yielded sharp peaks with a diameter is about 480 nm and at *p*H = 8.0 gives very sharp DLS with a diameter ~590 nm, which is greater by ~40 to 60 nm than the primary diameter and which is much larger than particular aggregates in SEM analysis (Fig. 6). Nonetheless, at *p*H 7.0, DLS displays broad peak with a diameter 865 nm, which support formation of inflatable aggregates (See, SEM images in Fig. 4). Nevertheless, DLS are in excellent agreement with the results obtained from SEMs, respect to the size and diameter of these assemblies of **OPP-1** were measured in acidic and basic aqueous water.

X-Ray Diffraction (XRD) study

X-ray diffraction (XRD) is a very useful method that offers chemical information for elemental analysis as well as for phase investigation. Besides chemical information characterization, XRD is extremely suitable for strain measurements as well as for surface analysis, which is a non-destructive method that offers inclusive information about the crystallographic structure which cannot be determined by single crystal structure also gives information of chemical composition, and also physical properties of materials. Samples to be analyzed using XRD must be crystalline, however, the technique can provide the degree of crystallinity in assembled supramolecular structures. X-ray diffraction (XRD) confirmed the crystallinity of **OPP-1** upon self-assembly in the both acidic and basic aqueous medium and did not exhibit any peaks in neutral *p*H, confirming that the material does not crystalize alone, thus, in full protonated form **OPP-1** is amorphous in nature. The strongest peak overlaps with pattern on amorphous silica signifying that **OPP-1** materials may consist of a mixture of several components present in different sizes in acidic and basic solutions. Herein, XRD technique was used to confirm the assembly of **OPP-1** at different *p*H values through characterize the crystallinity of aggregated states of **OPP-1**. As Fig. 8b is shown the XRD results of **OPP-1** in basic medium (blue-line), acidic medium (red-line) and neutral medium (black-line) from aqueous solution deposited on mediums. At both *p*H 5.0 and 9.0, there are three significant peaks were recorded at approximately 18°, 35°, 38° along with few small peaks, however, at *p*H 5.0 produces more broaden peaks as compared with *p*H 9.0 sharpening peaks were observed. This clearly confirming the crystallinity of assembled **OPP-1** in both acidic and basic medium. It is specific to mention that at *p*H 9, the XRD recorded four less intensive peaks at 31°, 45°, 53° and 55°. Furthermore,

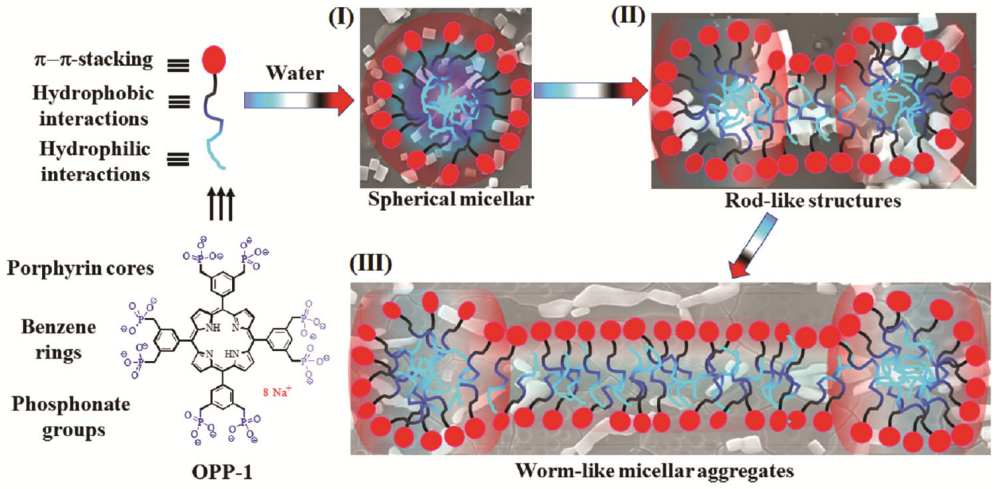

Fig. 9 — Schematic depiction of OPP-1 aggregates in aqueous solutions with varying *p*H ranging from 3.0-11.0. Typically, varying *p*H ranging from 3.0-9.0 structures formed include spherical micelles (**I**: *p*H = 8.0), rod-like micelles (**II**, *p*H 3.0-6.0), and worm-like micellar aggregates (**III**, *p*H 9.0-11.0), respectively.

the self-assembled of **OPP-1** at *p*H 5.0 (red line) displayed four lesser sharp peaks in between 30° to 35°. However, there aren't any peaks were observed at *p*H 7 (black-line), indicating the amorphous nature formed from neutral aqueous medium. These results clearly support the self-assembled supramolecules obtained from DLS analysis and SEM analysis of **OPP-1** at neutral, acidic and basic *p*H's from aqueous solutions, respectively.

Graphical illustration of OPP-1 with varying *p*H = 5.0-11.0

Schematic representation of **OPP-1** aggregates in aqueous solutions with varying *p*H ranging from 3.0-9.0 in these supramolecular structures formed include spherical micelles, rod-like micelles, and worm-like micellar aggregates, respectively. Schematic representation of **OPP-1** aggregates in aqueous solutions with varying *p*H ranging from 3.0-9.0 structures formed include spherical micelles (I: *p*H = 8.0), rod-like micelles (II, *p*H 3.0-6.0), and worm-like micellar aggregates (III, *p*H 9.0-11.0) are demonstrated in Fig. 9. The assembled supramolecules formation of **OPP-1** is due to not only π-π stacking of porphyrin core (red-globules) but also van Der Wall forces (hydrophobic aryl with methylene bridges) play major role in self-assembled structures and importantly hydrophilic interaction of phosphonate group of **OPP-1** interact with water *p*H dependently as illustrated by graphical representation in Fig. 9. Structures shaped varying *p*H ranging from 3.0 to 9.0 structures formed include spherical micelles (I: *p*H = 8.0), rod-like micelles (II, *p*H = 3.0 to 6.0), and worm-like micellar aggregates (III, *p*H 9.0-11.0), respectively. The SEM pictures were used as a background to compare with graphical illustrated self-assembled superstructures for comparative analysis.

Experimental Section

OPP-1 synthesis

Synthesis and characterization of **OPP-1** were prepared in six-steps with overall yield 21%, following our previous work[25].

Standard solution of OPP-1

Stock solutions (conc. 1×10^{-3} M) of **OPP-1** were made in water at *p*H 7.0 solution. For spectral measurements, this solution was injected into each time with 2 mL of water (varying *p*H) in a cuvette by micropipette.

Study of UV-Vis absorption and fluorescence spectroscopy

Stock solutions (~1×10^{-3} M) of **OPP-1** were prepared in water (*p*H = 7.0). A 0.2 mL aliquot of the stock solution was transferred to several different volumetric flasks in water at varying *p*H 3-11) and made each of 2 mL volume with addition of water (with maintaining *p*H values). The solutions were allowed to equilibrate for 2 h prior to the spectroscopic measurements. The most prominent features are a reduction in the peak intensity along with a significant red shift of the absorption maximum and a loss of the fine structure.

Scanning Electron Microscopy (SEM) analysis of OPP-1

The samples were characterized using a Scanning Electron Microscopy (SEM) using FEI Quanta 200 SEM (Royal Melbourne Institute of Technology (RMIT) University, Melbourne, Australia) operated at high voltage (HV) of 30 kV. Probes on silica wafer coating of **OPP-1** for enhanced reflectivity (NSC15/AIBS), with a typical resonance frequency of 325 kHz and a force constant of 40 N/m, were used for microscopy imaging. Sample on silica wafer surface of **OPP-1** were prepared by spin-coating the freshly prepared solution (1×10^{-4} M in water, at varying *p*H = 3.0 to 11.0) by silica coating at 2000 rpm and the solvent was allowed to bloated by filter paper before introduction into the vacuum system. Upon spin-coating and after few waiting for 2h remaining aqueous solution was removed by tapping with filter paper and images were collected. The width and length were accomplished by measure in micrometer of assembled supramolecules of **OPP-1**.

Conclusion

In summary, we have shown that by slight alteration of the *p*H ranging from 3.0-11.0, **OPP-1** self-assembled and form various supramolecular superstructures. Typically, at *p*H 7.0 formation of inflatable aggregates, *p*H = 5.0 produces spherical micelles which accumulate together to produce rod-like micelles and further in basic aqueous medium (*p*H = 8.0-9.0) yielded directional growth, similar to worm-like superstructures. However, in increasing *p*H to 11.0 worm-like structures combined together to form accumulated structures. The formation of self-assembled supramolecular superstructures due to complementary *H*-bonding of peripheral phosphonato group of **OPP-1** with partial deprotonated (acidic medium) form produces blue-shift (head-to-head: *H*-type arrangements) which is forbidden process because of lack of negative charges which produces short nanorods. However, fully deprotonated form *i.e.* in basic *p*H, **OPP-1** arranges head-to-tail (red-shift: *J*-type aggregates) which produces direction growth of the assembly in water. Formed self-assembly in the solution were investigated in solution *via* UV-Vis absorption, fluorescence spectroscopy. Furthermore, formed superstructures were visualize on silicon surface by SEM analysis. Importantly, deposition of **OPP-1** in varying *p*Hs ranging from 0.3-11.0 and even after spin coating and removing excess water, clearly shows stability of assembled structures. The key advantage of this technique is the additional control over precipitation process using the counterion. Moreover, the fully deprotonated in basic medium of **OPP-1** plays a crucial role in keeping the assembled structures apart in the solid state, preventing formation of non-fluorescent stacked dye aggregates, which was observed in more acidic (*p*H = 3.0-4.0) and more basic medium (*p*H = 11.0). Despite the clear compensations of this approach over the simple precipitation methods used for cationic porphyrins. Moreover, this method is obviously limited to ionic *i.e.* porphyrin bearing phosphonate functional groups. Nevertheless, it is useful method for the formation of worm-like structures with simply changing *p*H and very important to mention, we are currently studying interaction of **OPP-1** with cationic porphyrins as well as functionalization of core of **OPP-1** with zinc (II) and tin(IV) complexes in order to measure electric conductivities π-radical stacks will be reported in due course.[21]

Supplementary Information

Supplementary information is available in the website http://nopr.niscpr.res.in/handle/123456789/58776.

Author contributions

The manuscript was written through contributions of all authors. All authors have given approval to the final version of the manuscript.

Conflict of Interest

The authors declare that they have no competing financial interest.

Acknowledgments

SVB gratefully acknowledges UGC for the position of Professor under Faculty Recharge Programme and Central University Karnataka (CUK), Kalaburagi for proving adequate facilities.

References

1 Yoshimura S & Einaga Y, *J Phys Chem B*, 108 (2004) 15477.
2 Danino D, Abezgauz L, Portnaya I & Dan N, *J Phys Chem Lett*, (2016) 1434.
3 Yamashita Y, Maeda H & Hoffmann H, *J Colloid Interface Sci*, 299 (2006) 388.
4 P J Missel, N A Mazer, M C Carey & Benedek G B, *J Phys Chem*, 93 (1989) 8354.

5 Nettesheim F & Kaler E W, *Giant Micelles, Properties and Applications*, (Taylor and Francis, New York) 2007, p 41–79.
6 Ziserman L, Abezgauz L, Ramon O, Raghavan S R & Danino D, *Langmuir*, 25 (2009) 10483.
7 Dreiss C A, *Soft Matter*, 3 (2007) 956.
8 Sullivan P F, Panga M K R & Laffite V, *RSC Adv,* (2017) 330.
9 Danov K D, Kralchevsky P A, Stoyanov S D, Cook J L, Stott I P & Pelan E G, *Adv Coll Int Sci*, 256 (2018) 1.
10 Latterini L, Blossey R, Hofkens J, Vanoppen P, Schryver F C D, Rowan A E & Nolte R J M, *Langmuir*, 15 (1999) 3582.
11 Inamura I & Uchida K, *Bull Chem Soc Jpn*, 64 (1991) 2005.
12 Fuhrhop J H, Bindig U & Siggel U, *J Am Chem Soc*, 115 (1993) 11036.
13 (a) McDermott G, Prince S M, Freer A A, Hawthornthwaite-Lawless A M, M Papiz Z, Cogdell R J & Isaacs N W, *Nature*, 374 (1995) 517; (b) Roszak A W, Howard T D, Southall J, Gardiner A T, Law C J, Isaacs N W & Cogdell R J, *Science*, 302 (2003) 1969.
14 Drain C, Batteas J, Flynn G, Milic T, Chi N, Yablon D & Sommers H, *Proc Natl Acad Sci U S A*, 99 (2002) 6498
15 Tsuchida E, Komatsu T, Arai K , Yamada K, Nishide H & Fuhrhop J-H, *Langmuir*, 11 (1995) 1877.
16 Tsuchida E, Komatsu T, Arai K, Yamada K, Nishide H, Böttcher C, Fuhrhop J-H, *Chem Commun*, 10 (1995) 1063.
17 Komatsu T, Moritake M, Nakagawa A & Tsuchida E, *Chem Eur J*, 8 (2002) 5469.
18 Klyszcz A, Lauer M, Kopaczynska M, Böttcher C, Gonzaga F & Fuhrhop J-H, *Chem Comm*, (2004) 2358.
19 Napoli M De, Nardis S , Paolesse R, Vicente M, Lauceri R & Purrello R, *J Am Chem Soc*, 126 (2004) 5934.
20 Wang L, Liu H & Hao J, *Chem Comm*, 21 (2009) 1353.
21 Charvet R, Jiang D-L & Aida T, *Chem Comm*, (2004) 2664.
22 Rabe J P & Fuhrhop J-H, *J Am Chem Soc*, 119 (1997) 1660.
23 Porteu F, Palacin S, Ruandel-Teixier A & Barraud A, *J Phys Chem*, 95, (1991) 7438.
24 Lei S B, Wang C, Yin S X, Wang H N, Xi F, Liu H W, Xu B, Wan L J & Bai C L, *J Phys Chem B*, 105 (2001) 10838.
25 Bhosale S V, Kalyankar M B, Langford S J, Bhosale S V & Oliver R F, *Eur J Org Chem*, 2009 (2009) 4128.
26 Aljabri M D, Jadhav R W, Al Kobaisi M, Jones L A, Bhosale S V & Bhosale S V, *ACS Omega*, 4 (2019) 11408.
27 Jelley E E, *Nature*, 138 (1936) 1009.
28 Bricks J L, Slominskii Y L, Panas I D & Demchenko A P, *Methods Appl Fluoresc*, 6 (2018) 012001.
29 Renner C, Piehler J & Schrader T, *J Am Chem Soc*, 128 (2006) 620.
30 Fokkens M, Schrader T & Klarner F, *J Am Chem Soc*, 127 (2005) 14415.
31 Bhosale R S, Al-Kobaisi M, Bhosale S V, Bhargave S & Bhosale S V, *Sci Rep*, 5 (2015) 14609.
32 Gangemi C, Randazzo R, Fragala M, Tomaselli G, Ballistreri F, Tascano R, Sfrazzetoo G, Purello R & Urso A, *New J Chem*, 39 (2015) 6722.
33 Yamagata H, Maxwell D S, Fan J, Kittilstved K R, Briseno A L, Barnes M D & Spano F C, *J Phys Chem C*, 118 (2014) 28842.
34 Luo J, Xie Z, Lam J W Y, Cheng L, Chen H, Zhan X, Liu Y, Zhu D & Tang B Z, *Chem Comm*, (2001) 1740.
35 Liang J, Tang B Z & Liu B, *Chem Soc Rev*, 44 (2015) 2798.
36 Hong Y, Lam J W Y & Tang B Z, *Chem Soc Rev*, 40 (2011) 5361.
37 Yang Y, Cui J, Li Z, Zhong K, Jin L Y & Lee M, *Macromolecules*, 49 (2016) 5912.
38 Bhosale S V, Chintan J, Lalander C H & Longford S V, *Chem Comm*, 46 (2010) 973.